International Journal of Fatigue 64 (2014) 114–120

Contents lists available at ScienceDirect

International Journal of Fatigue

journal homepage: www.elsevier.com/locate/ijfatigue

Influence of different non-metallic inclusion types on the crack initiation in high-strength steels in the VHCF regime

D. Spriestersbach *, P. Grad, E. Kerscher

Materials Testing, University of Kaiserslautern, D-67663 Kaiserslautern, Germany

ARTICLE INFO

Article history:
Received 2 December 2013
Received in revised form 27 February 2014
Accepted 3 March 2014
Available online 12 March 2014

Keywords:
Very high cycle fatigue
Bainitic steel
Non-metallic inclusion
Fatigue crack initiation
Threshold value

ABSTRACT

This study aims to clarify the influence of different inclusion types on the crack initiation in the very high cycle fatigue regime. For this purpose ultrasonic tension–compression fatigue tests ($R = -1$) with the bainitic high-strength steel 100Cr6 (SAE 52100) were carried out until an ultimate number of cycles of 10^9. Additionally, runout specimens were tested repeatedly with higher stress amplitudes until failure occurred. By this method threshold values for the stress intensity factors in the very high cycle fatigue regime were found to be dependent on the inclusion type. So beside the threshold value for crack propagation of long cracks inside a fish-eye, K_{th}, another threshold value can be found for the formation of the so called fine granular area which is characteristic for very high cycle fatigue failure. This threshold value, below which no initiation in form of a fine granular area can be observed, is further dependent on the chemical composition of the crack initiating inclusion. Thus, a true fatigue limit in the very high cycle fatigue regime depends on the inclusion size and inclusion type. Further the inclusion type with the lowest threshold value indicates an absolute threshold value for very high cycle fatigue crack initiation due to the formation of the fine granular area.

1. Introduction

In recent years an increasing amount of research has been done to clarify the failure mechanism of high-strength steels in the very high cycle fatigue (VHCF) regime. By now it is well known, that high-strength steels do not show a classical fatigue limit and failure still occurs beyond 10^7 cycles [1–9]. The reason for such late failure is that the fatigue properties in the long life region are strongly affected by non-metallic inclusions inside the material [10]. As shown in [1–9] there is a transition of the fracture mode from surface-induced fracture to subsurface inclusion-induced fracture. Crack initiation in the VHCF regime (>10^7 cycles) mostly takes place at non-metallic inclusions inside the specimens and is accompanied by the formation of a ring-like fracture surface, the so-called fish-eye. At low stress amplitudes combined with very high numbers of cycles, a fine granular area (FGA) named by Sakai et al. [1] can be observed in the vicinity of an inclusion within the fish-eye. The FGA has also been observed by multiple researchers, so that various alternative names can be found in literature, such as optically dark area (ODA) [4], bright granular facet (GBF) [6] or rough surface area (RSA) [8] can be found. This study will use the term FGA by Sakai. Because of the great scientific interest a lot of different mechanisms for the formation of the FGA in the VHCF regime have been postulated [4,11–13]. Our study, however, seems to find answers to the following still open questions: How do different inclusion types influence the crack initiation within the FGA? Is there a threshold value for this FGA formation? If yes, what is the value below which FGA formation does not take place?

As inclusions inside the material act like stress raisers in the matrix the crack initiation and propagation during internal fracture is affected by the inclusion size and the applied stress amplitude. To evaluate the stress raising effect of an inclusion in the matrix it is helpful to use stress intensity factors (SIF). Based on the maximum applied stress σ_0 and the cross section *area* of the inclusion, measured on the fracture surface, the maximum SIF K_{max} can be calculated with the $\sqrt{area}$-model by Murakami [14] for internal inclusions as follows:

$$K_{max} = 0.5\sigma_0\sqrt{\pi\sqrt{area}}; \quad for \quad R = -1 \rightarrow K_{max} = \frac{\Delta K}{2} \tag{1}$$

This equation is independent of the inclusion's shape. The error is less than 5 % for elliptical defects and less than 10% for triangular or square defects [14]. Evaluations of the SIF of subsurface

* Corresponding author. Address: TU Kaiserslautern, Arbeitsgruppe Werkstoffprüfung, Gottlieb-Daimler-Straße, 67663 Kaiserslautern, Germany. Tel.: +49 (0)631 205 5536; fax: +49 (0)631 205 5261.

E-mail addresses: spriestersbach@mv.uni-kl.de (D. Spriestersbach), grad@mv.uni-kl.de (P. Grad), kerscher@mv.uni-kl.de (E. Kerscher).

http://dx.doi.org/10.1016/j.ijfatigue.2014.03.003
0142-1123/

inclusions at the point of crack initiation based on Murakami's equation lead to the conclusion that if the SIF of the inclusion is higher than a threshold value in the range of 4–6 MPa $m^{1/2}$ [1,7,8,11,15], the crack propagates by the formation of a fish-eye. In case of lower SIFs a FGA is formed in the vicinity of the inclusion. The crack within the FGA grows until the SIF at the edge of the FGA reaches of the above mentioned threshold value [1,7,8,11,15]. From this point on the crack grows by forming a fish-eye.

Most research works are based on the assumption that the different kinds of inclusions behave equally and accordingly there is no separation between different inclusion types [1,6–8,11, 16–18]. As a result, inclusions are only classified by size and independently of their chemical composition. In this context Murakami et al. [19] state that the chemical composition of the crack initiating inclusion is not the crucial factor controlling the fatigue limit. However, Murakami makes this conclusion for HCF-failure up to $2 \cdot 10^7$ cycles and it is questionable whether this statement is still true in the VHCF-regime. There is research about crack initiation at inclusions which indicates that this statement might not be suitable in the VHCF-regime and that here a differentiation of inclusion types is necessary. Monnot et al. [20] describe that although the size of inclusions does undoubtedly play an important role, the detrimental effect of inclusions depends not only on their size but also on their chemical composition. Their results show for instance that titanium nitride inclusions are about as harmful as inclusions containing aluminum oxide, although the latter are several times larger. Generally, inclusions of all types become more detrimental with increasing size. One reason why the types of the inclusions, that is their chemical composition, also influence the degree of harmfulness is seen in different damaging mechanisms causing the fatigue fracture. In this context Lankford and Kusenberger [21,22] as well as Furuya et al. [23,24] observed that spherical aluminium–silicium–manganese oxide and aluminium–calcium oxide inclusions in high-strength steels debond from the matrix during the first fatigue cycles and before a crack initiates from the matrix at the matrix/inclusion interface. In situ tensile and tension–compression observations of surface inclusions by Xie et al. [25] show a similar behavior for aluminium oxides resulting from a stress concentration under tensile loading at the matrix/inclusion interface. Local plasticity and inclusion debonding can be observed even below the macroscopic yield strength. In contrast, Zeng et al. [26] and Furuya et al. [23,24] discovered that for nearly cubic titanium nitride inclusions cracks start inside the inclusions. After crack initiation inside the inclusions the cracks penetrate the inclusion/matrix interface and propagate further into the matrix. In this case, the inclusions act as crack initiators and no debonding is observed. For elongated titanium nitride inclusions with a ratio of long to the short axes more than seven Zeng et al. [26] assumed that fatigue cracks likely occur at the inclusion/matrix interface. But it is visible that the pyramidal indentations for hardness measurement are so close to the observed inclusion that an influence of hardness indentations on the initiation cannot be excluded and that without these indentations all cracks might have initiated inside the inclusions. Bomas et al. [27] also observed these differences in crack initiation behavior between titanium nitride and calcium oxide inclusions. They noticed that titanium nitride inclusions break during loading while calcium oxide inclusions debond as mentioned by [21–25].

Similarly Tanaka and Mura [28] differentiate between three different types of crack initiation around inclusions. For the first type of initiation it is characteristic that the strength of the interface between inclusion and matrix is low enough to break during the first cycles without any plastic deformation. After this debonding the inclusion behaves like a void in the material and the crack initiates at the interface into the matrix. In the case of the second initiation mechanism, the interface does not break so that plastic flow is accumulated in the matrix and moving dislocations pile up at the inclusion until the inclusion breaks or debonds. If the inclusion does not break or debond, the crack can also initiate at a slip band emanating from the point of stress concentration. Providing that failure at different inclusion types is based on these different microstructural mechanisms of crack initiation, it is thinkable that these different mechanisms would also lead to varying thresholds and lifetimes for different inclusion types. This would mean that fatigue limit or fatigue life predictions can only be accurate if the appropriate fracture mechanisms for the destructive inclusions are taken into account. Although there are findings that the different kinds of inclusions behave differently during fatigue failure, there is nearly no differentiation in literature and the inclusion type is not regarded in anyway in models for the prediction of fatigue lives.

To fill this gap this work aims to clarify the influence of the different inclusion types on the crack initiation at non-metallic inclusions in the VHCF regime. In this context, it is of particular interest to find the basic initiation mechanisms and the resulting threshold values for crack initiation in the VHCF regime in dependency of the inclusion types.

2. Experimental procedures

2.1. Material and specimen

The material used in this study is the high carbon–chromium bearing steel 100Cr6 (material number 1.3505, similar to SAE 52100 or JIS SUJ2). The chemical composition is given in Table 1. The fatigue specimens have an hourglass-shape with a minimum diameter of 4 mm in the center and a stress concentration factor of 1.027 (see Fig. 1). They were manufactured from a rolled round bar with a diameter of 65 mm. In order to avoid segregations in the center of the bar the specimens were taken eccentrically. The specimens were machined in annealed condition with radial and axial oversize. Afterwards the specimens were austenitized for 20 min at 855 °C, cooled down rapidly and then hold for 7 h at 220 °C in a salt bath. This treatment results in a lower bainitic microstructure with an almost uniform hardness of 775 HV 10. Fig. 2 shows the resulting bainitic microstructure. After the heat treatment the specimens were manufactured into the final shape by cylindrical grinding. To remove residual stresses as a result of the grinding procedure the center of the specimen's gauge length was polished after the heat treatment. Furthermore, the lower surface roughness reduced the probability of crack initiation caused by surface defects which were created during the machining process.

2.2. Testing facility and procedure

Push–pull fatigue tests ($R = -1$) were carried out on an ultrasonic piezoelectric fatigue testing device at a frequency of about 20 kHz. The tests were performed in an open environment at room temperature. To prevent an abnormal heating of the specimens due

Table 1
Chemical composition of the tested 100Cr6 steel (in wt.% or ppm).

C	Cr	Si	Mn	P	S	Mo	Al	Cu	Ca	Ti
0.95	1.47	0.29	0.25	0.003	0.002	0.017	0.03	0.044	16 ppm	9 ppm

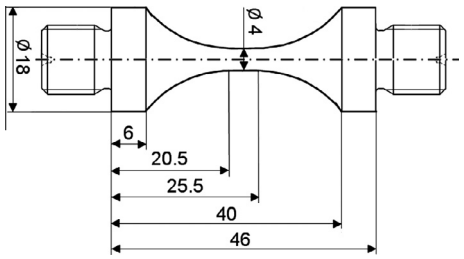

Fig. 1. Shape and dimension of the ultrasonic tension–compression fatigue specimen.

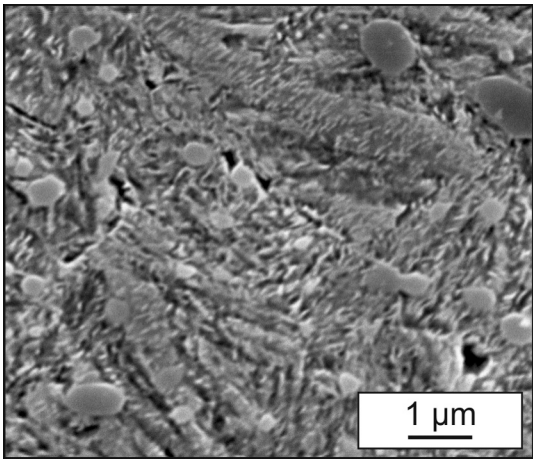

Fig. 2. SEM micrograph of the bainitic microstructure.

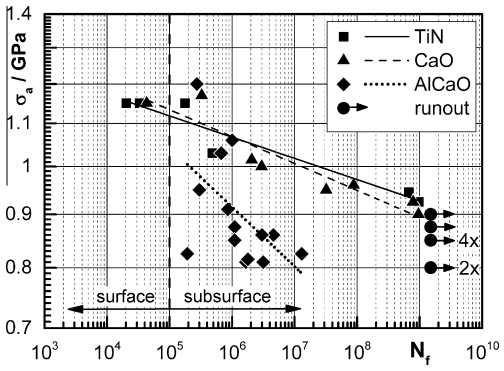

Fig. 3. *S–N* data obtained from axial loading fatigue tests ($R = -1$) classified into the different inclusion types.

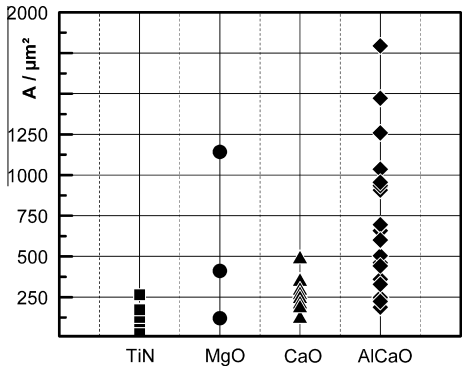

Fig. 4. Size distribution of the cross-section area of the different inclusion types.

to the high testing frequency the specimens were tested by ultrasonic pulse-pause cycles and additionally cooled with compressed air so that they did not heat up to more than 40 °C during the tests. The temperature was controlled by an infrared temperature sensor. Specimens which reached the ultimate number of load cycles of 10^9 were tested again. In these following tests the stress amplitude was increased by 50 or 100 MPa. If again no failure occurred after 10^9 cycles, this procedure was repeated until fracture occurred. The fracture surfaces of the failed specimen where then analyzed and measured with a scanning electron microscope (SEM), in addition, energy dispersive X-ray spectroscopy (EDX) was used to determine the chemical composition of the non-metallic inclusions at the fracture origin.

3. Results and discussion

Fig. 3 presents the *S–N* data of the push–pull fatigue tests sorted according to the crack initiating inclusion type. In general fracture always occurred due to non-metallic inclusions. The fatigue fracture at stresses below 1100 MPa and a fatigue life range higher than 10^5 cycles takes only place at non-metallic inclusions inside the material. At higher stress amplitudes and shorter life spans cracks initiate from inclusions at the surface of the specimen. If the fracture occurs because of a non-metallic inclusion under the specimen's surface two common kinds of fracture surfaces generally can be found: the fish-eye with and without a FGA in the vicinity of the crack initiating inclusion.

The inclusion types found in this study are mainly titanium nitrides (TiN), calcium oxides (CaO), aluminium–calcium oxides (AlCaO), magnesium oxides (MgO) and sometimes inclusions with a mixture of different types. Pure MgO inclusions were only observed during runout tests. The different kinds of inclusions are denoted in this paper by their main chemical components. The used notation does not reflect their exact chemical composition. The fatigue data shows a separation of the different inclusion types so that every inclusion type has its own *S–N* curve. The *S–N* curves for TiN and CaO are much clearer and provide less scatter relative to the fatigue than that for AlCaO. The size distribution for the different inclusion types in Fig. 4 indicates that the scatter in fatigue lives results from the scatter of the inclusion size found at the fracture surfaces. It can be seen that the cross-section area A of the inclusions in general range from 45 µm² for the smallest TiN up to 2700 µm² for the largest AlCaO found during the tests. AlCaO- and MgO-inclusions for instance are usually much bigger and provide a larger scatter than the other inclusion types. As a result fatigue fracture for those inclusions occurs at lower stress amplitudes than for TiN or CaO. Further it can be observed that no failure at AlCaO-inclusions occurs far beyond 10^7 cycles while TiN and CaO still cause fractures at nearly 10^9 cycles. Thus, the fatigue lives of the specimens in the VHCF regime seem to depend on the crack initiating inclusion type.

A closer look at the SIF at the inclusions in Fig. 5 shows that inclusions with a calculated SIF above the threshold value for propagation of a long crack K_{th} (for high strength steels $K_{th} \approx 4 - 6\text{MPa m}^{1/2}; K_{th} = \Delta K_{th}/2$ *for* $R = -1$) lead to a fish-eye fracture without FGA. The FGA formation occurs when the calculated value of the SIF falls below K_{th}. The SIFs resulting from the measured FGA size at the fracture surface show that as soon as the SIF at the edge of the FGA exceeds K_{th}, the formation of the FGA ends and the crack propagates forming a fish-eye. Further it becomes obvious that cracks at the observed inclusion types can initiate by building a FGA at different SIF-ranges. So for a ultimate number of load cycles of 10^9 cracks at AlCaO only initiate at a SIF

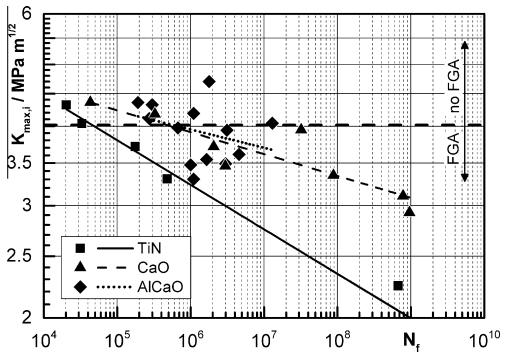

Fig. 5. SIFs for inclusions at the crack origin classified into the different inclusion types.

above 3.4 MPa m$^{1/2}$ whereas initiation still takes place at 2.9 MPa m$^{1/2}$ for CaO and even at 2.2 MPa m$^{1/2}$ for TiN. This indicates that the chemical composition of an inclusion might have a significant effect on the crack initiation at inclusions in the VHCF regime. The above mentioned fact that every inclusion type has a specific SIF, below which no failure occurs, might be an evidence for the existence of different threshold values for FGA formation in the VHCF regime at different kinds of inclusions and an ultimate number of load cycles of 10^9. We thus call these values $K_{th,FGA}$. An inclusion with a SIF under this specific threshold value $K_{th,FGA}$ will not lead to failure until 10^9 load cycles because no FGA formation is possible.

In order to specify this threshold, runout specimens were tested again with stress amplitudes increased by 50 or 100 MPa until fracture occurred. If the specimen reached 10^9 cycles with the higher stress the stress was raised again. All runout specimens tested in that way finally failed in the VHCF regime with FGA-formation on the fracture surface. Fig. 6 shows the results of the runout tests for bainitic and martensitic specimens (chemical composition and heat treatment from [15]) separated into the different inclusion types. The SIFs lying upon each other represent one additional runout test of the same sample. For each runout test the number of loads to failure at the last tested stress amplitude is shown. The fact that all runouts retested failed in the VHCF regime comparable to the lifetimes reached in the fatigue test at comparable SIFs leads to the assumption that damage accumulation can be neglected. The SIFs were calculated by using the measured inclusion sizes at the fracture surface and the applied stress amplitudes at each stress level. It is obvious that the fracture due to different inclusion types occurs in different SIF regions. The SIF values at the inclusions for the stress levels of the last unbroken and the broken

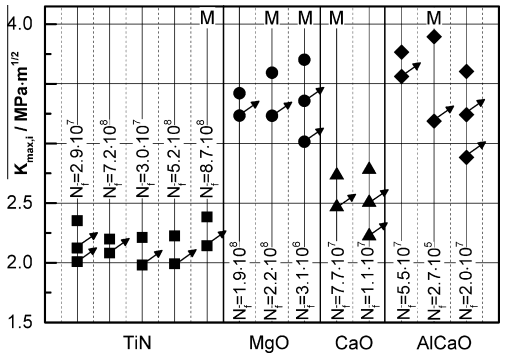

Fig. 6. SIFs at the different inclusion types of bainitic and martensitic runout specimens with the corresponding number of load cycles to failure at the last stress amplitude; martensitic runout specimen from [15] are marked with M.

test for each runout specimen indicate that there seems to be a threshold value for every inclusion type. The threshold value for crack initiation due to FGA formation for every inclusion type is given as the average of the mean values of the SIFs, which were calculated by the SIF of the last runout test at which a specimen still did not break and the SIF of the test at which this specimen failed. The thus calculated threshold values correspond quite well with the values determined by data from Fig. 5 (compare also Table 2).

Thus, under the assumption that a damage accumulation for runout specimens can be neglected the stress increase tests prove the existence of a dependency between inclusion type and threshold for FGA formation, as mentioned above in the observations on the fatigue tests. Fracture only occurred when the SIF at the inclusion exceeded the respective threshold for FGA formation. But it can be seen in Table 2 that the threshold value for AlCaO is slightly higher than the *S–N* data would suggest while the value for MgO fits well. In line with this, the fatigue tests represented in Fig. 5 shows only a few specimens with AlCaO-inclusions fracturing below the specific threshold for AlCaO as defined in the runout test. The concerned inclusions were all classified as AlCaO-inclusions but they all contain additionally a certain amount of MgO at their boundaries, which cannot be neglected. For instance Fig. 7 shows the results of an EDX-analysis of one of the AlCaO inclusions, at which fractured was initiated below the specific threshold value. Because of the position of the MgO at the edge of the inclusion where the debonding and crack initiation takes place and the lower threshold value for FGA formation, in this case, the threshold value of MgO rather than that of AlCaO seems to be critical for the crack initiation. Similarly a runout specimen with an inclusion which contained both CaO and MgO fractured at the threshold of MgO. Hence, in the case of mixed inclusions, which contain more than one inclusion type, it is not always clear which part of the inclusion is responsible for crack initiation and which threshold has to be taken into account. Generally it seems that MgO has a big influence if it is positioned at the boundary of an inclusion with a higher threshold value.

These differences in the initiation behavior of the different kinds of inclusions are a result of the varying properties of the inclusions and their interaction with the steel matrix. In general, the crack initiating inclusions found in this study can be divided into two groups: heterogeneous and homogeneous inclusions. At heterogeneous inclusions, like AlCaO, MgO or some CaOs for instance, the chemical components are not homogeneous distributed inside the inclusion. These inclusions have spherical shape and show a low bonding force to the matrix. Most fracture surfaces of such inclusions showed a clean gap between the inclusion and the matrix (see Fig. 8a). As visible in Fig. 8b, it happened that bigger parts or even the whole inclusion were missing at the crack origin in the fracture surface. During loading heterogeneous inclusions detach or decay so that the inclusion finally acts like a void in the material. The conditions in which these inclusions were found at the points of crack initiation confirm this behavior (see Fig. 8a–c). In this context the FEM simulations in Fig. 9, based on material data provided by [29–33] and the flow curve of the tested material, show the stress concentration K_t in relationship of the

Table 2
Comparison of the threshold values for the different inclusion types resulting from S-N data (Fig. 5) and runout test (Fig. 6).

Inclusion	$K_{th,FGA}$ from *S–N* data (MPa m$^{1/2}$)	$K_{th,FGA}$ from runout tests (MPa m$^{1/2}$)
AlCaO	3.4	3.56
MgO	–	3.4
CaO	2.9	2.62
TiN	2.2	2.17

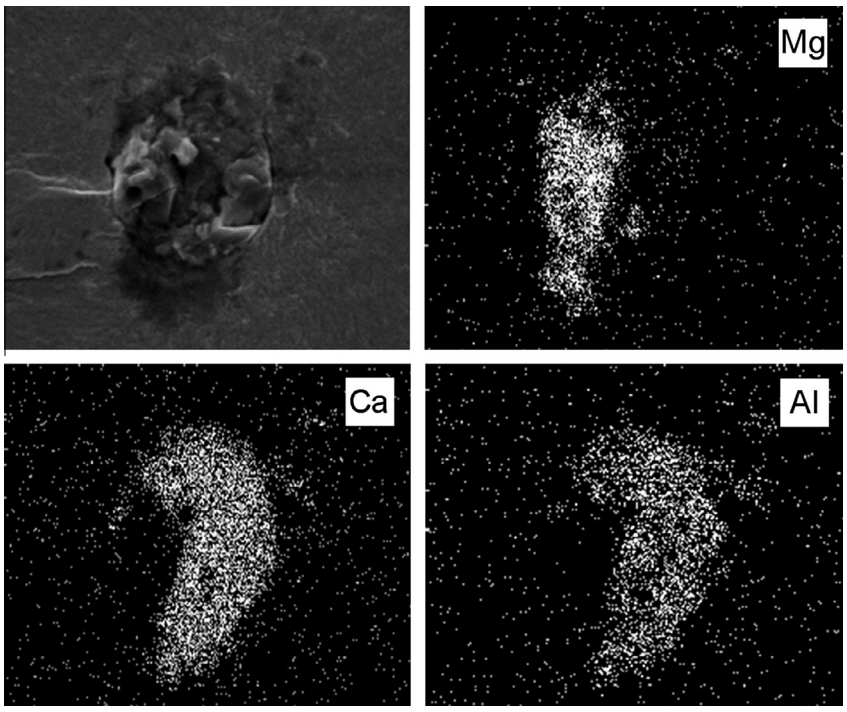

Fig. 7. EDX-analysis of AlCaO-inclusion broken below the $K_{th,FGA,AlCaO}$ determined by runout tests.

ratio x/r_i, where r_i is the inclusion diameter and x the distance to the center of the inclusion [34]. The maximum of the stress concentration K_t for elastic–plastic deformation behavior at a void can be localized in the matrix at the equator of the inclusion. As a result, the crack at heterogeneous inclusions has to initiate at the equator of the void, where the stress concentration reaches its maximum, before it can propagate into the steel matrix. The void can provide several initiation sides so that multiple cracks can initiate at the equator of inclusion/matrix interface. For this reason, heterogeneous inclusions show up to five crack layers on the fracture surface near the inclusion (see Fig. 8a–c). With increasing crack propagation inside the fish-eye the different crack layers fuse into one dominant crack layer. Because of the similar fracture mechanisms inclusions like AlCaO, MgO and CaO lead to

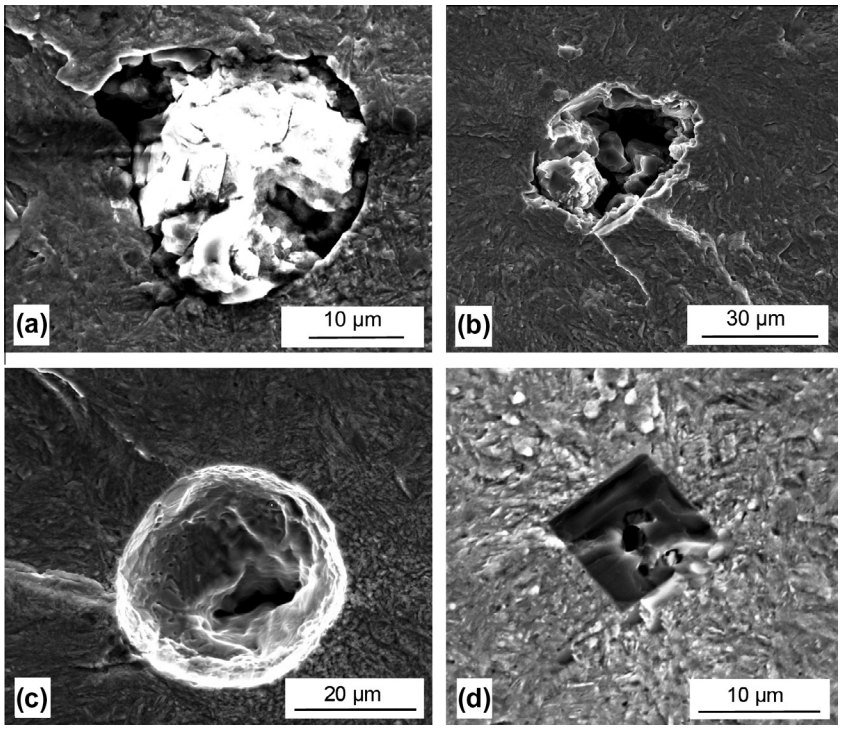

Fig. 8. (a) Debonded AlCaO-inclusion; (b) leftovers of a broken AlCaO-inclusion; (c) void left over after an AlCaO-inclusion separated from the matrix with different crack layers; (d) broken TiN-inclusion with another small globular inclusion in its center.

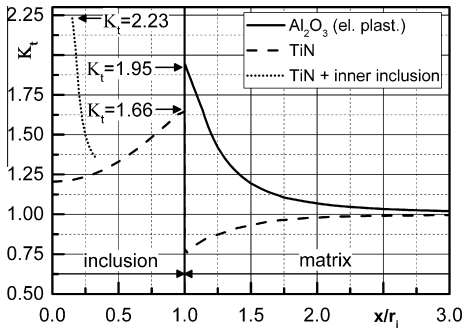

Fig. 9. Calculated stress concentration factors K_t around AlCaO-inclusions for elastic plastic material response in bainite and TiN-inclusions.

comparable threshold values. The debonding of the spherical CaO-inclusions seems to be possible at lower stress concentrations and thus result in a lower $K_{th,FGA}$. But maybe the fact that their structure is sometimes more homogeneous also affects their threshold value.

Inclusions with a homogeneous structure like TiNs which have a sharp-edged cubic morphology and are tightly bound to the matrix, behave differently during fatigue fracture. The stress concentration K_t for TiN has its maximum inside the inclusion and not in the matrix. If the TiN-inclusion contains another small inclusion in its center (see Fig. 8d) the maximum of the stress concentration of $K_t = 2.23$ can be found at the edge of the inner inclusion (see Fig. 9 dotted line). Without this inner inclusion the maximum has a value of $K_t = 1.66$ and lies at the inclusion matrix interface inside the inclusion (see Fig. 9 dashed line). This stress concentration inside the inclusion causes an early cracking of the inclusion after a few load cycles. This is the reason why the fracture at homogeneous inclusions starts inside the brittle inclusion rather than in the matrix and forms a sharp crack. If the SIF at the inclusion is higher than the respective threshold for FGA formation this crack can propagate across the inclusion/matrix interface into the matrix and form a FGA. As a result, such cracks can initiate at much lower SIF's in comparison to those initiated by inclusions with a weaker bonding to the matrix, which mostly show only one crack layer rarely two (see Fig. 8d). It becomes apparent that with increasing homogeneity the initiation behavior changes and as a result the threshold values changes too.

Thus, if damage accumulation can be neglected, the experimental results show that the fatigue limit is dependent on the inclusion type. This makes it possible to calculate a critical inclusion diameter for the different inclusion types and a ultimate number of cycles of 10^9 for a given load [34]. Under the assumption that for homogeneous inclusions, like TiN, a perfect crack is initiated, which then grows into the surrounding matrix, it might be possible to take the threshold for TiN as the absolute threshold for crack initiation caused by FGA formation. The crack propagation at such a crack during VHCF failure is only possible if an adequate dislocation movement takes place at the crack tip. In this context Weertman [35] used the following equation to calculate a SIF below which no dislocation movement is possible:

$$K_{th,Weertman} = \frac{1}{2}\Delta K_{th,Weertman} = \frac{1}{2} 2gE\left(\frac{2b}{5}\right)^{1/2} \quad (2)$$

With $b = 2.5 \cdot 10^{-10}$ m, $E = 212$ GPa and $g = 1$ a threshold with a value of $K_{th,Weertman} = 2.1$ MPa $m^{1/2}$ for body-centered materials results from this equation. This is in line with the threshold found during the fatigue tests of homogeneous TiN inclusions which provide a nearly perfect sharp crack tip. This value thus could be seen as an absolute threshold value for FGA formation. Li et al. [36] proposed a similar value for an absolute fatigue threshold $K_{th} = 2.47$ - MPa $m^{1/2}$. The higher threshold values for heterogeneous inclusion can be explained by the fact that when the inclusions debond, they act like a hole in the material where a crack still has to build while homogeneous TiN-inclusions break during the first loads and provide instantly perfect sharp cracks.

4. Conclusions

The ultrasonic fatigue tests show that VHCF failure is highly dependent on the different types of inclusions in the material. The fatigue fracture caused by inclusions inside the material can be divided into two general groups: fractures initiated at sharp cracks formed from homogeneous inclusions like TiN and fracture initiated at voids in the material resulting from broken or detached heterogeneous inclusions, as for example AlCaO. Threshold values for VHCF failure of high-strength steel by FGA-formation at the different kinds of inclusions inside the material can be found in ultrasonic fatigue test up to 10^9 cycles and additional runout test. These threshold values are dependent on the characteristics of the inclusion and the interaction between the inclusion and the surrounding matrix. Thus, it can be concluded that every type of inclusion has its own threshold value for crack initiation by FGA formation in the VHCF regime. These specific threshold values for FGA-formation, as determined by runout tests, lie at 3.56 MPa $m^{1/2}$ for AlCaO, at 3.4 MPa $m^{1/2}$ for MgO, at 2.62 MPa $m^{1/2}$ for CaO and go down to 2.17 MPa $m^{1/2}$ for TiN. Furthermore the threshold of TiN-inclusions that break during the first loads and provide nearly perfect cracks seems to represent an absolute threshold for fatigue failure. This value is in line with results of Li et al. [36] and calculations of Weertman [35].

Acknowledgement

This research was carried out in the framework of the Deutsche Forschungsgemeinschaft (DFG) priority program 1466 Infinite Life. The authors would like to thank the DFG for the financial support of this work.

References

[1] Sakai T, Sato Y, Oguma N. Characteristic *S–N* properties of high-carbon–chromium–bearing steel under axial loading in long-life fatigue. Fatigue Fract Eng Mater Struct 2002;25:765–73.
[2] Shiozawa K, Hasegawa T, Kashiwagi Y, Lu L. Very high cycle fatigue properties of bearing steel under axial loading condition. Int J Fatigue 2009;31:880–8.
[3] Bathias C, Drouillac L, Francois PL. How and why the fatigue *S–N* curve does not approach a horizontal asymptote. Int J Fatigue 2001;23:143–51.
[4] Murakami Y, Nomoto T, Ueda T. Factors influencing the mechanism of superlong fatigue failure. Fatigue Fract Eng Mater Struct 1999;22:581–90.
[5] Shiozawa K, Lu L. Effect of non-metallic inclusion size and residual stresses on gigacycle fatigue properties in high strength steel. Adv Mater Res 2008;44–46:33–42.
[6] Shiozawa K, Lu L, Ishihara S. *S–N* curve characteristics and subsurface crack initiation behaviour in ultra-long life fatigue of a high carbon–chromium bearing steel. Fatigue Fract Eng Mater Struct 2001;24:781–90.
[7] Tanaka K, Akiniwa Y. Fatigue crack propagation behaviour derived from *S–N* data. Fatigue Fract Eng Mater Struct 2002;25:775–84.
[8] Ochi Y, Matsumura T, Masaki K, Yoshida S. High-cycle rotating bending fatigue property in very long-life regime of high-strength steels. Fatigue Fract Eng Mater Struct 2002;25:823–30.
[9] Bayraktar E, Garcias IM, Bathias C. Failure mechanisms of automotive metallic alloys in very high cycle fatigue range. Int J Fatigue 2006;28:1590–602.
[10] Murakami Y. Metal fatigue: effects of small defects and nonmetallic inclusions. Oxford: Elsevier; 2002.
[11] Shiozawa K, Morii Y, Nishino S, Lu L. Subsurface crack initiation and propagation mechanism in high-strength steel in a very high cycle fatigue regime. Int J Fatigue 2006;28:1521–32.
[12] Sakai T, Harada H, Oguma N. Crack initiation mechanism of bearing steel in high cycle fatigue. In: 16th European conference of fracture, Alexandroupolis; 2006. p. 1129–30.
[13] Grad P, Reuscher B, Brodyanski A, Kopnarski M, Kerscher E. Mechanism of fatigue crack initiation and propagation in the very high cycle fatigue regime of high-strength steels. Scr Mater 2012;67:838–41.

[14] Murakami Y, Kodama S, Konuma S. Quantitative evaluation of effects of non-metallic inclusions on fatigue strength of high strength steels. I: Basic fatigue mechanism and evaluation of correlation between the fatigue fracture and the size and location of non-metallic inclussions. Int J Fatigue 1989;11:291–8.
[15] Grad P, Kerscher E. Fatigue crack paths in the VHCF-regime of 100Cr6. In: 4th International conference on crack paths. Italy; 2012. p. 401–8.
[16] Liu YB, Yang ZG, Li YD, Chen SM, Li SX, Hui WJ, et al. Dependence of fatigue strength on inclusion size for high strength steels in very high cycle fatigue regime. Mater Sci Eng A 2009;517:180–4.
[17] Bathias C. Gigacycle fatigue of bearing steels. Mater Sci Technol 2012;28.
[18] Lu LT, Zhang JW, Shiozawa K. Influence of inclusion size on *S–N* curve characteristics of high-strength steels in the giga-cycle fatigue regime. Fatigue Fract Eng Mater Struct 2009;32:647–55.
[19] Murakami Y, Toriyama T, Koyasu Y, Nishida S. Effect of chemical composition of nonmetallic inclusions on fatigue strength of high strength steels. ISIJ 1993;79:678–84.
[20] Monnot J, Heritier B, Cogne JY. Relationship of melting practice, inclusion type, and size with fatigue resistance o bearing steels. In: Effect of steel manufacturing processes on the quality of bearing steels; 1988. p. 149-165.
[21] Lankford J, Kusenberger FN. Initiation of Fatigue Cracks in 4340 Steel Metallurgical. Transactions 1973;4:553–9.
[22] Lankford J. Initiation and early growth of fatigue cracks in high strength steel. Eng Fract Mech 1977;9:617–24.
[23] Furuya Y, Hirukawa H, Kimura T, Hayaishi M. Gigacycle Fatigue Properties of High-Strength Steels According to Inclusion and ODA Sizes. Metall Mater Trans A 2007;38A:1722–30.
[24] Furuya Y, Matsuoka S, Abe T. A novel inclusion inspection method employing 20 kHz fatigue testing. Metall Mater Trans A 2003;34A:2517–26.
[25] Xie X, Zhang L, Zhang M, Dong J, Bain K. Micro-mechanical behavior study of nonmetallic inclusions in P/M disk superalloy RENE'95. Superalloys 2004;451–458.
[26] Zeng Y, Fan H, Xie X. Effects of the shape and size of rectangular inclusions on the fatigue cracking behavior of ultra-high strength steels. Int J Miner Metall Mater 2013;20:360–4.
[27] Bomas H, Linkewitz T, Mayr P. Analyse der Ermüdungsrissbildung und Dauerfestigkeit des Stahles 100Cr6 im bainitischen Zustand. HTM 2002;57:190–8.
[28] Tanaka K, Mura T. A theory of fatigue crack initiation at inclusions. Metall Mater Trans A 1982;13A:117–23.
[29] Brooksbank D, Andrews KW. Stress Fields around Inclusions and Their Relation to Mechanical Properties. J Iron Steel Inst 1972;21:246–55.
[30] Brooksbank D, Andrews KW. Tessellated stresses associated with some inclusions in steel. J Iron Steel Inst 1969;207:474–83.
[31] Brooksbank D, Andrews KW. Thermal expansion of some inclusions found in steels and relation to tessellated stresses. J Iron Steel Inst 1968;206:595–9.
[32] Acht C, Dalgic M, Hunkel M, Irretier A, Lübben T, Surm H. Ermittlung der Materialdaten zur Simulation des Durchhärtens von Komponenten aus 100Cr6 Teil1. J Heat Treat Mater 2008;63:234–44.
[33] Bauccio M. ASM engineered materials reference book. Mater Park OH 1994.
[34] Grad P. Rissinitiierung und rissausbreitung im VHCF-bereich des hochfesten stahls 100Cr6. In: Schriftenreihe der Arbeitsgruppe Werkstoffprüfung. TU Kaiserslautern. Kaiserslautern; 2013.
[35] Weertman J. Fatigue crack growth in ductile metals. In: Mechanics of fatigue: Presented at the winter annual meeting of the American Society of Mechanical Engineer, Washington, DC; 1981.
[36] Li W, Sakai T, Li Q, Lu LT, Wang P. Effect of loading type on fatigue properties of high strength bearing steel in very high cycle regime. Mater Sci Eng A 2011;528:5044–52.